JGISE Vol. 6 No. 2 (2023), pp. 136 - 152 | https://doi.org/10.22146/jgise.88002

JGISE
Journal of Geospatial Information Science and Engineering
ISSN: 2623-1182 | https://jurnal.ugm.ac.id/jgise

Examining the spatio-temporal relationship between LST, NDVI, NDBI and LULC change of Pachhua dun, Dehradun, Uttarakhand (India)

Rahul Thapa[1], Vijay Bahuguna[1], Prateek Negi[2], Praveen Singh Rana[1], Pinki Kataria[1], Geeta Rawat[3], Muhammad Yasir[4], Tania Sharma[1]

[1]D.B.S.(P.G.) College, Dehradun (Uttarakhand) , India
[2]Pestle Weed College of Information Technology, Dehradun, Uttarakhand, India
[3]SGRR University, Dehradun, Uttarakhand, India
[4] China University of Petroleum, India

Corresponding : Rahul Thapa **| Email:** Rahulthapa126@gmail.com

Diterima (*Received*): 16/Aug/2023 Direvisi (*Revised*): 19/Nov/2023 Diterima untuk Publikasi (*Accepted*): 22/Nov/2023

ABSTRACT

Recent climate change has had a negative impact on a wide range of human and natural systems, and it is clear that humans influence the climate. Because, as anthropogenic influence increases, the heat output from the land surface increases, speeding up the rate of climate change. In this regard, the use of RS and GIS techniques has provided various opportunities for research to examine these changes. The current analysis is based on the Landsat 1989, and 2020. Over the study period of 31 years, the built-up regions increased in size from 44.23 km^2 to 154.56 km^2. Whereas, the area covered by scrubland, water bodies, and vegetation cover has significantly decreased. The LST study further supports the outcome, showing that the mean and standard deviation increased from 14.81°C±1.32(1989) to 18.82°C±1.57(2020). The study also made an effort to examine how LULC affected LST; while vegetation cover has consistently helped to lower mean LST, built-up areas and scrubland are the main drivers of mean LST rise. The LST and NDBI revealed a positive correlation, while the NDVI/SLOPE and LST showed a negative correlation. Subsequently, the multiple linear regression (MLR) models concluded that the BUAs has evolved into a serious threat to the increase in LST, but increase in vegetation cover and SLOPE would result in slight decrease in LST. the study recommended that the government create policies that restrict future land encroachment and conversion, notably of forested area and water bodies, and make an immediate effort to increase the quantity and quality of urban green cover in the study area. So that we may, respectively, minimize the potential hazard posed by future LST rise and LULC change.

Keywords: Supervised classification; LULC; Change detection; LST and urban green.

1. Introduction

In recent decades, a wide range of advancements in land use and land cover change (LULCC) methods and techniques have been developed, along with a variety of mapping techniques for measuring LULCC using change detection technique (Darius, 2017; Lv et al., 2018; Mishra et al., 2020). In this regard, LULCC are crucial indicators while understanding human activities and environmental interactions (Dewan et al., 2012). It is essential to obtain current and accurate LULCC data in order to interpret and analyse the environmental effects of such change because the straightforward change detection technique is rarely sufficient in and of itself (Giri et al., 2005; Srivastava et al., 2012). However, the primary fundamental factor determining the LULC change regarding pattern and size remains alike for most urban areas, i.e., "population growth", such changes are continuous and dynamic. Nevertheless, the growth of urban and suburban regions demands additional land and encourages the transformation of rural areas into urban areas (Xiaoqing & Jianlan, 2007). The imperative for urbanization and the demand for increased human settlements frequently give rise to an inescapable consequence: the irreversible loss of functional and natural land cover. This phenomenon, in turn, leads to localized alterations in temperature, weather patterns, and precipitation, thus sparking intricate environmental dynamics with potential far-reaching implications (Morshed et al., 2022; Sresto et al., 2022a). When these changes are concentrated over large areas, they have the

potential to affect the Earth's climate by altering local, regional, and global circulation patterns, altering the reflectance of the Earth's surface, and raising the atmospheric CO_2 concentration (Fattah et al., 2021; Sresto et al., 2022a). As a result, growing urbanisation reduces environmentally friendly land cover types like forests, vegetation, scrubland, and water bodies, which has an impact on the ecosystem and, consequently, carbon sequestration (Fattah et al., 2021). This effect ultimately contributes to climate change and global warming, as well as a rise in LST (Morshed et al., 2022; Sresto et al., 2022b; Thakur et al., 2020). Considering the method of classification, the supervised classification method was used in the area of interest to determine the LULCC Classification and accuracy assessment of each classification algorithm (Verma et al., 2020). When calculating the surface energy budget, evaluating the LULCC, and investigating other aspects of the earth's surface, the land surface temperature (LST) is an essential element and an indispensable factor(Guha et al., 2020a), the conversion of the marshland primarily influences the LST increase into agricultural land or bare land; and the conversion of the vegetation cover into the built-up area (BUAs)(Mallick et al., n.d.). In contrast to vegetated areas, impermeable surfaces shift the momentum balance between the LST and surrounding atmosphere, which changes heat exchange patterns (Jana et al., 2020a). Numerous previously published studies and numerous scientists from various areas proved that LULC has an influence on LST (Guha & Govil, 2021; Pal & Ziaul, 2017a; J. A. Sobrino et al., 2001; Santosa, 2016). Regarding NDVI, the research into the correlation between LST and LULCC aids in the resolution of problems pertaining to man - nature interactions and climate change, as the vegetation in the area determines the LST by evapotranspiration through the latent heat influx from the surface to the atmosphere (Jha et al., 2000). Since LST has a significant impact on land unitization management systems, the correlation between LST and NDVI in research involving remote sensing is extremely significant (Guha et al., 2020a; Guha & Govil, 2020). The LST-NDVI relationship is influenced by a wide range of variables, including the climate, vegetation types, land use, urbanisation, etc (Guha et al., 2020b). The relationship between LST and NDVI has been calculated in numerous earlier research (L. Chen et al., 2013; Deng et al., 2018; Fatemi & Narangifard, 2019; Guha et al., 2020a). The normalised differential build-up index (NDBI), on the other hand, measures the amount of impervious surface in BUAs, one of the main forms of land cover. It can be used as a measure of the intensity of development (Macarof & Florian, 2017; Syafitri & Santosa, 2020), several earlier studies have demonstrated that BUAs land can quicken the land's LST (Amiri et al., 2009; Song et al., 2014; Yuvaraj, 2020). Therefore, suggested that the LST change is a crucial criterion for assessing the environmental quality and socio-economic development policies (Guha & Govil, 2020; Jalan & Sharma, 2014; Malik et al., 2019; J. Sobrino et al., 2004). Given the significance of slope in response to LULC, NDBI, and NDVI. The LULC change and slope can be related, and this relationship has important consequences for a variety of environmental and socioeconomic issues. Slope, in fact, influences anthropogenic (agricultural, urbanisation, infrastructure) development through determining the level of soil erosion, water runoff patterns, vulnerability, and natural hazards. Therefore, slope is frequently observed as the major element in land cover changes (Çetin, 2019). Additionally, the statistical approaches such as regression analysis can aid in assessing the degree and direction of a correlation between LULC change and slope. Several studies have indicated that topographical features such as slope, elevation, and aspects influence the spatial distribution and spread of vegetative cover (Walsh et al., 2001), LULC, NDBI and NDVI.

Recent developments in R.S. and G.I.S. tools have enabled researchers to detect and analyse such changes more efficiently (Bhat et al., 2017), so that more precise research outcome data could be obtained. Several previous studies on the temperature trends of Dehradun city and Doon Valley (Agarwal et al., 2019; Jana et al., 2020a; Patidar & Sankhla, 2015; Taloor et al., 2020) have also highlighted the cause and consequences of LST rise. The major purpose of this study is to determine the NDVI, SLOPE, and NDBI values by employing change detection; to identify the area of change and by analysing the spatiotemporal variation in LULC, LST, NDVI, and NDBI; to evaluate the strength of the association between LST and NDVI, SLOPE, and NDBI using the correlation coefficient (r). Finally, a multiple linear regression model was developed to determine the predictor and its significance for the LST. The model's prediction aids in interpreting how LST changes in response to NDVI, SLOPE, and NDBI changes.

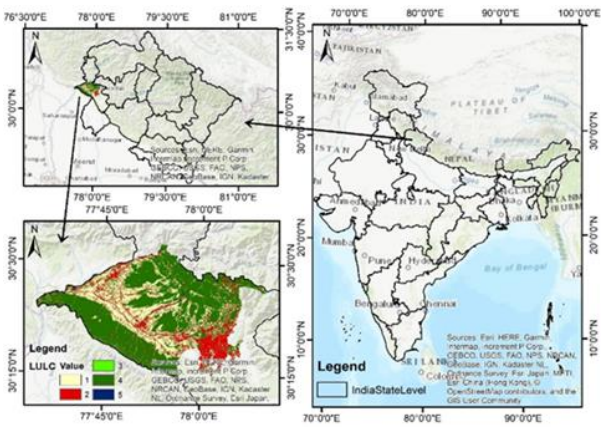

Fig. 1 Location of the Area of Interest (AOI).

2. Map of the Study area

The study area of the current research was situated in the western part of the Dehradun district, Uttarakhand, India. The study area has a longitudinal extent of 77°34'30"E to 78°10'30''E, and the latitudinal extent is

30°13'30''N to 30°32'30"N as shown in Fig. 1, and its elevational range varies from 362m to 2320m from the mean sea level. The research area for the current analysis includes Pachhua Dun (Vikasnagar and Sahaspur) and the Dehradun urban agglomeration (DUA) as illustrated in Figure 1 showing the location of the area of interest.

The study area's average annual precipitation is 2073.3 mm, and the months of June through September account for the majority of the district's yearly precipitation (Government of Uttarakhand, 2022). As per the Census 2011, the total population of Sahaspur andVikasnagar C.D Block was 167501 and 153793 persons respectively; and the total population of Dehradun Municipal Corporation (DMC) was + Out Growth (OG) was 5,74,840, and the total population of Mussoorie urban agglomeration was 33657.

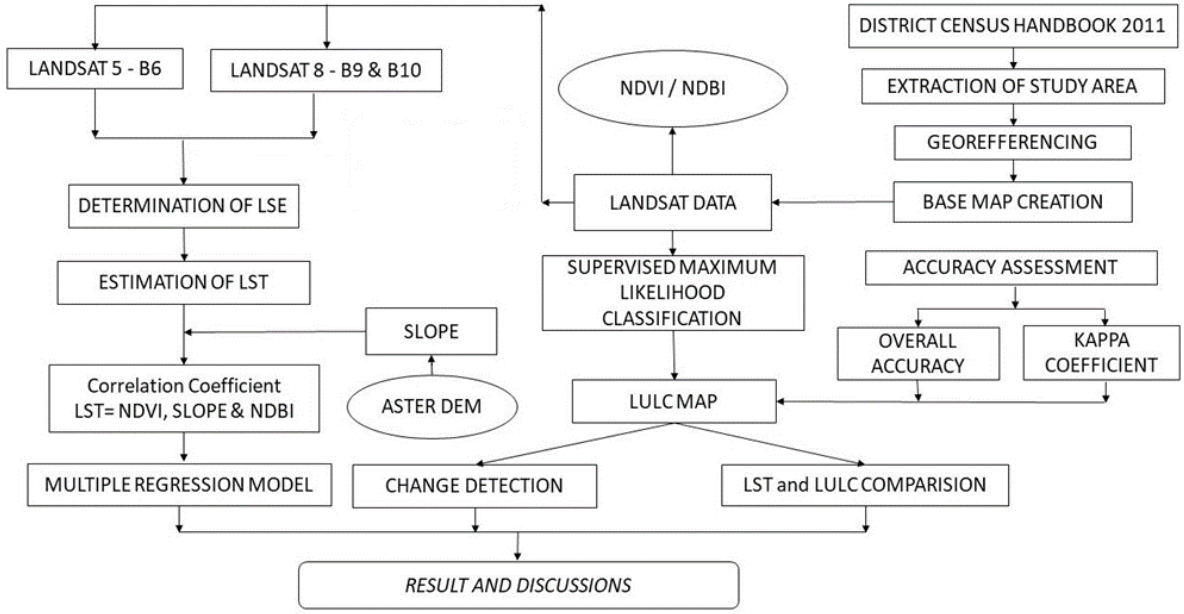

Fig. 2. Flow chart of research methodology.

Table 1. Data sources and Method of Data Collection

Data types	Data Sources	Method of data collection	Date of Aq.
Landsat-5 TM, 1989	http://earthexplorer.usgs.gov/	Download (with path and row no.146 by 39)	1989/12/05
Landsat 8 OLI/TIRS, 2020	http://earthexplorer.usgs.gov/	Download (with row and path no. 147 by 39)	2020/12/10
AOI and Population data	District Census Handbook 2011	*censusindia.gov.in*.	2022/11/02
SRTM DEM	http://earthexplorer.usgs.gov/	N30E077, N30E078	2022/05/12

3. Material and Methods

For the purpose of mapping the LULC change of study area, which includes polygons of Pachhua Dun including the urban agglomerations of Dehradun and Mussoorie, Landsat-5 TM satellite images from the years 1989 and 2010, as well as a high-resolution cloud-free 10 per cent Landsat 8 OLI/TIRS, 2020 image, have been chosen. Fig. 2 shows the methodological framework employed for the study, while Table 1 gives more information on data collection methods and data sources.

3.1 Method and techniques of Landsat image classification

The most popular approach for image classification used to extract LULC classes and create LULC maps is maximum likelihood classification (MLC). It was carried out using the MLC tool available in ArcGIS 10.8, a supervised classification method(Ahmad & Quegan, 2012). Since it bases its classifications on Bayes' classifications, it calculates the statistical probability for each LULC category while taking into consideration the covariances and variances of the training sample data classes. The software ArcGIS 10.8 was extensively used to detect changes from 1989 until 2020. The numerous LULC classes in the study area are then divided into five main categories: AL, BUAs, O/SL, VC, and WB. Table 2 highlights a description of each of the five LULC classification schemes.

3.2 Change detection technique

The change detection technique recognizes gaps in the state of a phenomenon or an object by examining it at a

distinct period (author et al., 2004). Therefore, in order to achieve the best resource management, it is important to regularly, timely, and accurately apply change detection techniques on the Earth's surface. This forms the foundation for higher-quality, in-depth analysis. Change detection has become an essential technique for managing and monitoring the progress of urban growth and natural resources (Hassan et al., 2016). The last few decades have witnessed growth in various change detection methods viz., Post-classification comparison technique, change matrix, image differencing, and principal component analysis (author et al., 2004). In the current paper, the vital information about the spatial distribution of LULCC is presented by the post-classification change matrix (Shalaby & Tateishi, 2007); subsequently, the error-matrix has represented LULCC to assess the overall LULCC generated from classified images of the study area.

3.3 LST, NDVI, NDBI and SLOPE extraction

a. Extraction of LST from Thermal Band

The Digital Number (DN) is converted into the Spectral Radiance (Lλ) from Landsat 5 and Landsat 8. The sensor radiance could be transformed according to the signals obtained by thermal sensors. Each object is capable of discharging thermal electromagnetic energy. As indicated in Eq.(1)(Aakriti & Ram, 2015; Nichol & To, 2012).

$$L_\lambda = M_L * Q_{cal} + A_L \quad (1)$$

Table 2. Description of different LULC classification schemes used.

Class	General description
AL	Agricultural fallow Land and irrigated Agricultural Land.
BUAs	Human Settlements and Roads
O/SL	Agroforestry, Shrubs, Land with tree canopy density (10-40 per cent).
VC	Land with tree canopy density 40 per cent >
WB	The area under Perennial and Ephemeral rivers.

Where (Lλ) is a Top of Atmosphere (TOA) spectral radiance (Watts/m2 × srad × μm), ML is the multiplicative scaling factor for band-specific radiance, QCAL is the DN of given Pixel (Band 6,10 and 11), and AL is the band-specific additive rescaling factor. In terms of constant value, Landsat 5-1989 TM, and Landsat 8, 2020 has constant values for Band 10 (K1) and (K2) of 774.88 and 1321.08, as well as in B11 (K1) and (K2) of 480.88 and 1201.14 respectively.

b. Calculating Land Surface Emissivity LSE ($\boldsymbol{\varepsilon}$)

The surface emissivity ranges between 0.97 and 0.99, and it was estimated using the (J. Sobrino et al., 2001) as given in Eq. (4)

$$\varepsilon = 0.004_{P_v} + 0.986 \quad (4)$$

Where, ε = Land surface emissivity (LSE); Pv = Proportion of vegetation, According to Carlson and Ripley (Carlson & Ripley, 1997), Pv for both Landsat 5 and Landsat 8 image could be derived from NDVI image, as given in Eq. (5)

$$P_V = \left(\frac{NDVI_{max} - NDVI_{min}}{NDVI_{max} - NDVI_{min}}\right)^2 \quad (5)$$

Where:
$NDVI_{max} = Min\ DN\ values\ from\ NDVI\ image$, and
$NDVI_{min} = Max\ DN\ values\ from\ NDVI\ image$.

c. Land Surface Temperature

Second, the (Lλ) was converted into a satellite brightness temperature(BT) Kelvin T(K) using Eq. (6) derived from the following formula (Weng et al., 2004).

$$LST(K) = \frac{T_r}{In\varepsilon(\frac{\lambda * \mathrm{Tr}}{p}) + 1)} \quad (6)$$

Where, λ = central wavelength (in μm) of the Landsat thermal band; p was derived using Eq. (6) = 1.438*10-2 m K. Thus, LST, NDVI and NDBI images derived have been used to study Spatio-temporal patterns; and h = Planck's constant (6.26 × 10-34 J·s), S= Stefan Boltzmann's constant (1.38 × 10-23 J·K-1), c= Velocity of light (2.998×10-8 m/s and p= 14380), Ɛ = denotes the surface emissivity(Zhou & Wang, 2011a) However, even after the emissivity correction, the temperature stays almost the same(Lo & Quattrochi, 2003; Nzoiwu et al., 2017).

$$p = \frac{h \times c}{s}(1.438 \times e^{-2}\, mK) \quad (7)$$

d. Conversion of Kelvin into degrees Celsius

The thermal band converted Kelvin (K) into degrees Celsius (°C) using Eq. (8)

$$T(℃) = T - 237.15 \quad (8)$$

e. NDVI (Normalized Difference Vegetation Index)

The greenness of the environment is measured by NDVI (Lo & Quattrochi, 2003), and the NDVI is calculated through the data acquired in NIR and Red band of Landsat satellite using Eq.(2) given by (Rouse et al., 1973)and Eq.(2a) for Landsat 8.

$$NDVI\ (Landsat\ 5) = \frac{NIR - Red}{NIR + Red} \quad (2)$$

$$NDVI(Landsat\ 8) = \frac{Band5 - Band4}{Band5 + Band4} \quad (2a)$$

Where for Landsat 5, the Red (B3) and NIR (B4) are the spectral reflectances of vegetation in the red and infrared bands. In Landsat 8, the Red (B4) and NIR (B5) represent vegetation in red and infrared bands.

f. Normalized Difference Built-up Index (NDBI)

The NDBI is also considered an essential factor of LST to identify urban and built-up areas (Zha et al., 2003), It is an indicator of urban areas that can uncover built-up and barren land (Thomlinson et al., 1999), and it could be derived using Eq.(3 and 3a).

$$NDBI\ (Landsat\ 8) = \frac{SWIR1 - NIR}{SWIR1 - NIR} \quad (3)$$

$$NDBI(Landsat\ 5) = \frac{BAND5 - BAND4}{BAND5 + BAND4} \quad (3a)$$

g. Digital Elevation Model (DEM): SLOPE

A three-dimensional (XYZ) digital cartography dataset called a "Digital Elevation Model" (DEM) is created using photogrammetric or contour line methods (Gandhi & Sarkar, 2016). However, the ASTER sensor from the Terra satellite, which is available to 99 percent of the world for free and offers elevation data with a 30m resolution, was employed for the current investigation. The SLOPE value was then extracted from the ASTER DEM using ArcGIS 10.8.

3.4 Accuracy Assessments

Accuracy assessment plays a significant role in any classification project as it seeks to quantitatively assess the effectiveness of the sampled pixels in the correct LULC classes. The Kappa coefficient, overall accuracy (OvAc), producer accuracy (PrAc), and user accuracy (UsAc) were used as instruments in the accuracy assessment. Thereafter, an accuracy evaluation of all MLC-classified images was made using an error matrix (Pal & Ziaul, 2017b; Yusuf et al., 2014; F. Zhang et al., 2016; Y. Zhang et al., 2013). Where the UsAc is the percentage of sampled pixels accurately categorised inside the satellite image, showing the "Error of Commission," and the PrAc reflects the likelihood that a sampled pixel is classified to a LULC type and represents the "Error of Omission." The ratio between the total number of training pixels that were properly detected and the total number of pixels used for accuracy evaluation is then used to calculate OvAc. The objective is to have an overall accuracy of 85 per cent, with no LULC class having an accuracy below 70 per cent (Thomlinson et al., 1999).

a. Overall Accuracy (OvAc)

The OvAc is a ratio between correctly classified training pixels and the total number of pixels as given in Eq. (9)

$$OvAc = \frac{OvAc \sum_{a=1}^{u} c_{aa}}{Q} \times 100\% \quad (9)$$

Where the lowest acceptable OvAc is 85 and Q and U are the total numbers of training pixels and Class, respectively. The (K) was used in conjunction with an OvAc assessment to get results with greater precision.

b. Kappa Coefficient(K)

The agreement between two sets of the categorical dataset is measured by (K) while correcting for chance agreement between the categories(Jenness & Wynne, 2005). (K) was considered for calculating the classification system's performance(Rogan & Chen, 2004) for LULC. (K) report the relationship between the reference data and the classified map (Lillesand et al., 2015). (K) the statistic measures agreement on a scale where 0.00 indicates agreement being no better than chance or there is no correlation in the classification, whereas a (K) of 1 represents perfect agreement. Interpretation (Landis & Koch, 1977) of (K), and its formula are given in (Table 3) and Eq. (10).

$$K = \frac{n\sum_{i=1}^{p} x_{ii} - \sum_{i=1}^{p}(x_{i+} \times x_{+i})}{n^2 - \sum_{i-1}^{p}(x_{i+} \times x_{+1})} \quad (10)$$

Where, p = Number of classes, $\sum x_{+1}$= $\sum$ of column i; and $\sum x_{i+}$ = $\sum$ of row i, and n = Total number of training pixels, and $\sum x_{ii}$ = Total number of elements of the error matrix. In order to represent the results, the error matrix was then built by comparing the reference class labels for the LULC class with the actual results(Stehman & Czaplewski, 1998).

Table 3. Interpretation of Kappa coefficient (K)(Landis & Koch, 1977)

Sr. No	Kappa	Interpretation
1.	< 0	No Agreement
2.	0.0 - 0.20	Slight Agreement
3.	0.21 – 0.40	Fair Agreement
4.	0.41- 0.60	Moderate Agreement
5.	0.61-0.80	Substantial Agreement
6.	0.81-1.00	Almost perfect agreement

Source: Landis and Koch (1977)

3.5 Correlation Coefficient and Multi-Linear Regression Model.

a. Correlation Coefficient (r)

The correlation (r) is an indicator of the strength of the linear relationship between the two different variables, as far as the strength of the relationship (Naidoo et al., 2013) of (r) is concerned, 0.00- 0.2 is regarded as a very weak; 0.2-0.4 is weak or low; 0.4-0.7 is moderate; 0.7-0.9 as strong and high strength of relationship; and 0.9-1.0 is interpreted as a very strong and very high strength of the relationship. Eq. 11 (Yim et al., 2010) is as follows;

$$r = \frac{\Sigma XY - \frac{(\Sigma X)(\Sigma Y)}{N}}{\left(\Sigma X^2 - \frac{(\Sigma X)^2}{N}\right)\left(\Sigma Y^2 - \frac{(\Sigma Y)^2}{N}\right)} \quad (11)$$

Where X denotes the independent variables, and the dependent variable is given as Y. and n is the number of observations. Furthermore, to test the strength of the relationship, the formula of the correlation coefficient of determination is given in Eq.12 below;

$$C/D = r^2 \quad (12)$$

Where C/D represents the Coefficient of determination; and r^2 is denoting the Correlation coefficient (Awuh et al., 2019).

b. Multiple linear regression (MLR)

Using a variety of explanatory variables, the MLR statistical method forecasts the outcome of a response variable. It is also known as multiple regression, the MLR can be viewed as an extension of simple linear regression (SLR), where there are p explanatory variables, or SLR can be thought of as a particular case of MLR p=1. The value of LST, NDVI, SLOPE, and NDBI were statistically analyzed for the creation of a model using, MLR with the help of SPSS 25 (Yuvaraj, 2020), the formula is given in Eq. 13 below;

$$Y = \alpha + \beta_1 x_1 + \beta_2 x_2 + \beta_3 x_3, \quad (13)$$

Where the dependent variable is Y, and α is the intercept, $\beta_{1,2,3..,}$ are independent variables which would be the predictor of the dependent variables.

3.6 Accuracy assessment of the raster layers

Table 4. Statistical summary of accuracy assessment of LULC map

LULC Class	Landsat 5 - 1989		Landsat 8 - 2020	
	User%	Producer%	User%	Producer%
AL	75.96	75.24	87.42	88.59
BUAs	64.39	87.63	88.29	89.50
O/SL	83.82	71.25	72.22	72.22
VC	92.16	87.85	96.17	97.10
WB	85.00	80.00	84.68	80.15
OvAc	79.42%		87.46%	
Kappa (K)	74.08%		84.04%	
Com. errors	20.35%		14.24%	
Om. errors	19.73%		14.75%	

#OvAc=Overall Accuracy

#Com. Errors=Commission Errors; Om. Errors =Omission Errors

Table 4 represented the statistical summary of the accuracy assessment results and exhibits the OvAc, Kappa (k), commission errors, and omission errors in detail. The OvAc and (K) values were 79.42 per cent and 74.08 per cent for the Landsat 1989, which falls in between the 0.61-0.80 range of kappa statistics, Thereby the strength of agreement for this classified image turns out to be a Substantial Agreement. However, the OvAc was 87.46 per cent, and the kappa statistics value was 84.04 per cent for Landsat 8, 2020. Which falls in between the 0.81-1.00 range of (K); thus, the strength of agreement for this Landsat 8 image turns out to be an Almost Perfect Agreement.

3.6.1 Conversion matrix of LULC map

Tables 5 and 6 exhibit the details of the net Loss/Gain area and the percentage covered by each class. Fig 3 and 4 show the final result obtained from the analysis of change detection of each LULC class. The 1989 to 2020 period analysis revealed that a significant amount of LULCC occurred in the area.

Table 5. Temporal Change dynamics of Area under each LULC Class of AOI (1989 and 2020.

LU/LC Categories	1989		2020	
	Area Km²	Area %	Area Km²	Area %
AL	256.82	27.58%	248.86	26.74%
BUAs	44.23	4.75%	154.56	16.61%
O/SL	72.90	7.83%	9.87	1.01%
VC	526.70	56.57%	511.99	55.01%
WB	30.37	3.26%	6.81	0.73%
Total Area	*931.01*	*100%*	*930.97*	*100 %*

The agricultural land with a total area of 256.82 km2 dominates the significant proportion compared to BUAs, which covered merely 4.75 per cent (44.23 km2) of the geographical area in 1989. Whereas the vegetation cover occupied the most extensive land cover area with 56.57 per cent (526.70 km2) of the study area. The study's overall analysis from 1989 to 2020 indicated that the study area had registered a fast expansion in the BUAs with an overall growth of +249.45 per cent (110.33 km2). Population growth has long been seen as a significant contributor to LULCC, because rising urbanization, and population pressure have led to the expansion of Dehradun (the number of wards has increased from 60 to 100 in 2018)(Dehradun Nagar Nigam, 2018). The expansion of BUAs is considered to be strongly tied to population increase and rising socio-economic development (Fanan et al., n.d.) both of which have long been recognized as important drivers of LULC changes (Chamundeeswari, 2013).

Table 6. Detail matrix of Net Loss/Gain of each land use and land cover change

LU/LC Categories	1989-2020	
	Area in Km²	Percentage
AL	-07.96	-03.10%
BUAs	+110.33	+249.45%
O/SL	-63.03	-86.46%
VC	-14.71	-02.79%
WB	-23.56	-77.58%

On the other hand, the open scrubland and water bodies registered; negative growth of -86.45 per cent (-63.03 km2) and -77.58 per cent (-23.56 km2) respectively, the loss of open scrubland and vegetation cover area was mainly attributed to the growth of agricultural land and BUAs expansion, and the newly BUAs were explicitly developed in the sub-urban zones; BUAs and open scrubland primarily replaced the areas

previously covered by agricultural land and open scrubland but located at a lower altitude and around the primary roads. The water bodies had witnessed an overall negative growth of -77.56 per cent (-23.55 km2) of land cover, and it mainly got converted into BUAs followed by agricultural land and open scrubland. Simultaneously, the vegetation cover and agricultural land; both classes have registered a total loss of -2.79 per cent (-14.71 Km2) and -3.1 per cent (-7.96 km2) accordingly. The most of area of open scrubland has been largely changed into agricultural land and BUAs and exhibits the strong influence of anthropogenic activities.

4. Result and Discussions

4.1 Land use and land cover change detection

For the LULC change study, a total of five land area classifications were used, namely agricultural land (AL), built-up areas (BUAs), open scrubland (O/SL), vegetation cover (VC) and waterbodies (WB) have been considered, and the supervised MLC technique was applied for the in-depth LULC change analysis. According to Table 4, the accuracy assessment was conducted using the kappa coefficient (k) and overall accuracy (OvAc). It determined that the overall accuracy in 1989 was 79.42 per cent and 87.46 per cent in 2020. While the kappa values were 74.08 and 84.02 per cent respectively. This suggested that the highest possible level of classification accuracy was established. Tables 5 to 6 provide a statistical overview of the LULCC in the Pachhua dun, Mussoorie, and DMC. The results showed that, between 1989 and 2020, a significant portion of the Agricultural land area had been converted into BUAs. At the same time, vegetation cover and open scrubland have been largely converted into agricultural land before it gets converted into built-up, supported by (Agarwal et al., 2019; Gupta, n.d.; Jana et al., 2020a; Patidar & Sankhla, 2015; Taloor et al., 2020; Thapa & Bahuguna, 2021). Based on the results statistics, the major development is directly associated with uncontrolled rapid urbanization and population growth, which further demands land use for several anthropogenic activities like residential, commercial, industrial, and infrastructural development and other concrete-led development. The special economic zone area - Selakui industrial zone of Pachhua dun, and Dehradun urban areas provides better job opportunities and standard of living, educational, healthcare facilities to the many people of nearby villages, blocks, districts, and states. Subsequently, this situation motivates people to temporary or permanent migration. As a result, most of the plain areas of doon valley especially areas of agricultural land, open scrubland, water bodies and vegetation cover, are highly subjected to developed projects and converted into built-up areas. The housing prices are cheaper than the city's core in the peri-urban areas and rural area, therefore becomes a preferred choice of residential locations for various income groups and social classes.

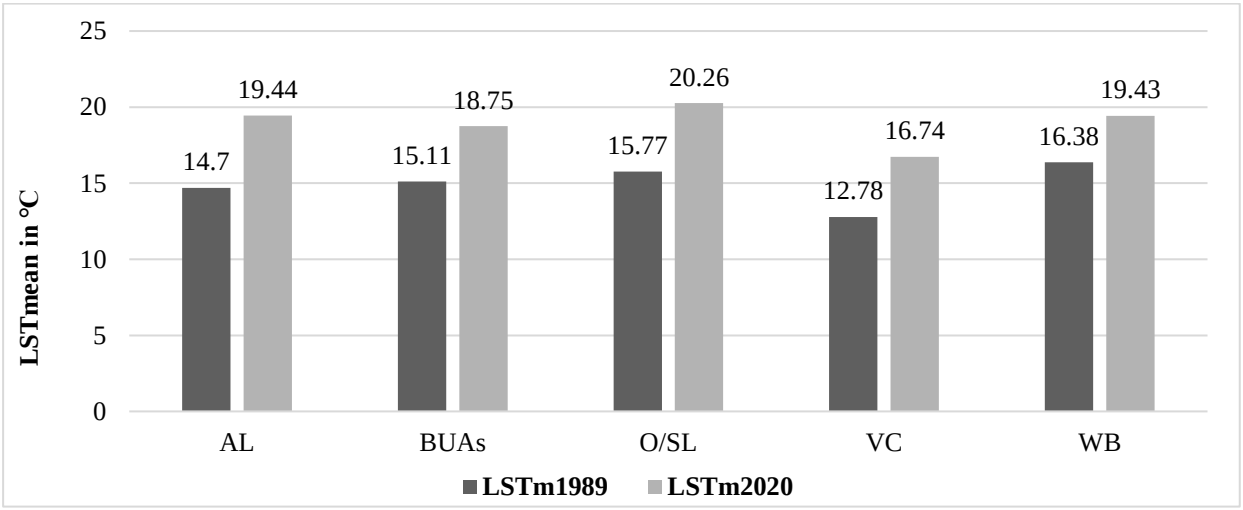

Fig. 3 Column graph exhibiting LST mean of the LULC classes of 1989 and 2020

4.2 LULC change and its influence on LST.

Fig. 3 illustrates the bar graph exhibiting LST mean of the LULC classes of 1989 and 2020. The data extraction of LST, NDVI, NDBI and SLOPE was obtained using fishnet (sample representation) tool available in ArcGIS 10.8. A total of 1185 points were generated within the polygon of the area of interest. The result obtained from the Landsat satellite images showed that the mean LST and standard deviation (SD) value for Landsat 1989 image was 13.79°C±2.02 and 17.86°C±2.04 for Landsat 2020 image. Overall, the area of interest has registered the growth of 4.07°C±0.02 respectively. Five land use and land cover classes agricultural land, built-up areas, open scrubland, vegetation cover and waterbodies have been considered to correlated with LST conditions. In the first observation period of year 1989, the maximum LST value was retrieved from open scrubland (20.48°C), followed by vegetation cover (20.04°C) and water bodies (19.16°C). Whereas the minimum LST was retrieved from vegetation cover (5.50°C) and agricultural land (10.40°C). On the other hand, the maximum LST value for 2020 was retrieved from vegetation cover (23.17°C)

followed by agricultural land (22.73°C) and BUAs (22.54°C). Furthermore, the minimum LST value was retrieved from vegetation cover (9.26°C), followed by BUAs (9.57°C) and agricultural land (16.37°C) as illustrated in the Table 7 exhibiting the statistical summary of spatio-temporal variation in LST in °C.

Table 7. Statistical summary of Spatio-temporal variation in LST in °C

Year	LULC	Range	Min	Max	Mean	σ
1989	AL	7.86	10.40	18.26	14.70	1.28
	BUAs	4.14	13.23	17.37	15.11	0.82
	O/SL	8.18	12.30	20.48	15.77	1.06
	VC	14.54	5.50	20.04	12.78	1.90
	WB	5.93	13.23	19.16	16.38	1.32
Average LST 1989		14.98	5.50	20.48	13.79	2.02
202	AL	6.36	16.37	22.73	19.44	1.20
	BUAs	12.97	9.57	22.54	18.75	1.63
	O/SL	2.95	18.82	21.77	20.26	1.17
	VC	13.91	9.26	23.17	16.74	1.78
	WB	5.92	16.20	22.12	19.43	2.20
Average LST 2020		13.90	9.26	23.17	17.86	2.04

Overall, the result of the first observation period 1989 revealed that the waterbodies (16.38°C±1.32) had the highest mean LST value (1989), followed by open scrubland (15.77°C±1.06) and BUAs (15.11°C±0.82). However, vegetation cover (12.78°C±1.90) had the lowest mean LST followed by agricultural land. On the other hand, for the year 2020, open scrubland (20.26°C±1.17) had the greatest mean LST, followed by agricultural land (19.44°C±1.20) and water bodies (19.43°C±2.20), while vegetation cover (16.74°C±1.78) had the lowest mean LST, followed by BUAs (18.75°C±1.63). Hence the result explicitly shows that vegetation cover was continuously aided in reducing mean LST values in the study area, as the vegetation induces more evapotranspiration; it is associated with vegetation greening. Consequently, a strongly influencing the local climatic conditions. It is also important to mention that the vegetation can also warm local temperatures by reducing albedo(Christopher et al., 2007; J.C., 1990). The result of the analysis, also reveals that the mean LST values have registered a noticeable increase, primarily due to more considerable LST fluctuation retrieved from BUAs. Which is a paved surfaces that tend to absorb solar radiation for longer periods, hold infrared radiation longer, and retain heat for extended periods than other LULC classes(Liu & Zhang, 2011; Lu et al., 2020).

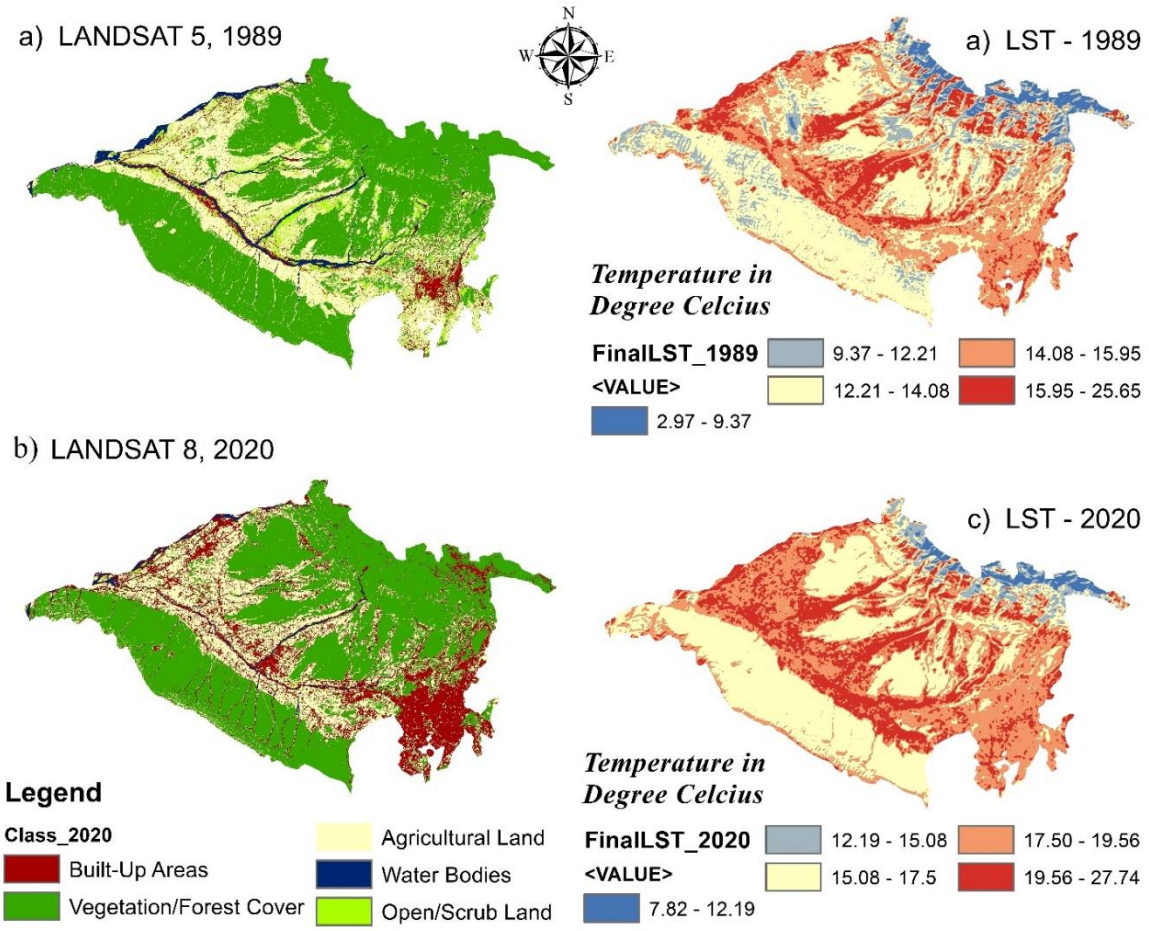

Fig. 5 spatio-temporal variation (1989 and 2020) in LST and LULC in the Selakui region of Pachhua dun. (A) Colour Infrared image of Landsat 1989 and 2020 (B) Map of LULC change (C) Map of LST change

4.3 LST difference in each LULC class in 1989 and 2020.

Fig. 4 illustrates the comparison between the Landsat satellite images of 1989 and 2020 using Composite band, LULC and LST image; and Fig. 5 depicts the spatio-temporal variation of LST and LULC in the Selakui region of study area. Additionally, Table 8 exhibits the Statistical summary of the mean LST difference in each LULC class, The mean LST was computed for each LULC class over the analysed period using Landsat 1989 and 2020. It was apparent from the result that the LULC classes influences LST values, i.e., LST change depends on LULC units. Therefore, investigating each LULC class's thermal signatures is essential to comprehend the relationship between LULC and LST (Weng et al., 2004). The study results show that the spatial extent, pattern, and intensity of mean LST have increased outwards from the city's core in all directions. Despite the fact that the area of interest is predominantly covered with vegetation and agricultural land, the results also showed that the LULC changing pattern of the research areas significantly contributes to the variance of LST. However, the overall period of analysis from 1989 to 2020 gave us the final clear picture of the LST change that occurred to the LULC change. The result revealed that the highest mean LST rise was registered in agricultural land by 4.70°C, followed by open scrubland (4.29°C) and vegetation cover (3.95°C), considering the agricultural land usually has higher LST than BUAs(Kumar et al., 2017), the lowest the mean LST rise was registered in water bodies and the BUAs by 3.19°C and 3.91°C. The highest mean LST difference was recorded in agricultural land by 4.70°C, followed by open scrubland and vegetation cover by 4.29°C and 3.95°C. The lowest mean LST difference was recorded in water bodies and BUAs by 3.19°C and 3.91°C. After state formation on 09-11-2000, the study area has witnessed a significant rise in anthropogenic activities, primarily the rapid expansion of BUAs caused by population rise and urbanization but at the expense of agricultural, open scrubland, waterbodies and vegetation land. Fig. 4 compares the Landsat satellite images of 1989 and 2020 of the Selaqui region (Sahaspur C.D. Block) of the Pachhua Dun, using RGB band combinations, LULC, and LST map. It is evident from the figure 5 that, during Landsat 1989 image analysis, the LST retrieved from the Selaqui region was majorly between 15°C - 18°C, however, in 2020 the LST value retrieved from the same region increased significantly, and now it primarily fell between 18°C-21°C. The mean LST value retrieved from the BUAs was 15.16°C in 1989, and 19.07°C. In agricultural land, it has exhibited a mean LST value of 14.76°C, and 19.46°C in 1989, and 2020 respectively, and registered a growth of 4.70°C mean LST between 1989-2020. Such high mean LST value experienced by open scrubland, ephemeral river bed, and agricultural land indicates that the radiation-exposed soil and Land have greater thermal properties and emit energy, which contributes to the warming of the environment. Thus, the analysis achieves consistency and coherence with the result obtained by Jana et al.(Jana et al., 2020b). In the study area, the evapotranspiration (ET) surfaces such as agricultural land, open scrubland, and vegetation cover were primarily replaced by non- (ET) surfaces like BUAs in LST increase between 1989-2020. Conversion of vegetation increases CO_2 accumulation in the atmosphere, which influences the surface energy budget(Islam & Islam, 2014),

Thereby results confirm the decreasing effect of (ET) surfaces (vegetation cover, agricultural land, open scrubland, and water bodies) and the increasing effect of non-(ET) surface-like BUAs on LST variations, which is also aptly highlighted in other studies(Amanollahi et al., 2016; Reisi et al., 2019; Singh et al., 2017). Additionally, to LULC's impact on LST increase, urban areas' population also increases LST by rising anthropogenic heat discharge(Zhou & Wang, 2011b). Hence waterbodies were not significantly contributed to minimizing LST during Dec, 1989 and 2020, as LST is sensitive to local moisture variations (L. Sun et al., 2013; Q. Sun et al., 2017); however, water bodies can regulate temperature as it helps in maintaining the atmospheric air circulation(Balew & Korme, 2020). The growth of BUAs at the expense of vegetation cover, agricultural land, open scrubland, and water bodies indicated that such expansion and LULCC would continue in the future. Similar findings were also observed by (Pal & Ziaul, 2017a), (Saini & Tiwari, 2017).

4.4 Correlation between NDVI and NDBI.

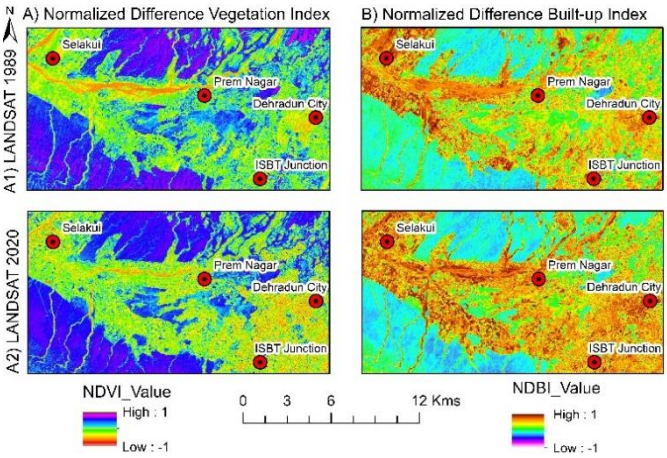

Fig. 6 spatio-temporal variation of NDVI and NDBI in the area of interest.

The result revealed that the Agricultural land and open scrubland both have registered high NDVI values other than vegetation cover. The mountainous areas of the Shivalik/lesser Himalayan range and other forested ranges within the research area have yielded the highest NDVI values. It is noteworthy that the mean NDVI value was less than 0.4 since the NDVI value during the winter months of December or January declined, grew, and

peaked during the summer month (June and July) (Naif et al., 2020). The conversion of the vegetation cover areas into BUAs, agricultural land or open scrubland results in an LST increase (Mallick et al., n.d.). Table 9 also illustrated that the mean NDBI and Standard deviation (SD) values in 1989 were 0.050±0.096 ranging from (-0.436) – (0.229); and for the year 2020 the mean and SD value of NDBI was -0.071±0.095 ranged from (-0.375)- (0.231). The area with high NDBI values was retrieved primarily around the Selakui, Kedarwala, Vikasnagar, and Dehradun city.

Table 8 Retrieved statistics values of LST, NDVI, and NDBI in the study area (1989-2020)

Variables	Year	Min	Max	Mean	SD
NDVI	1989	-0.172	0.600	0.311	0.164
	2020	-0.054	0.468	0.216	0.085
NDBI	1989	-0.292	0.342	0.024	0.160
	2020	-0.272	0.091	-0.105	0.081
LST	1989	5.497	20.481	13.789	2.020
	2020	9.265	23.169	17.860	2.040

Valid N = 1185; SD = Standard Deviation

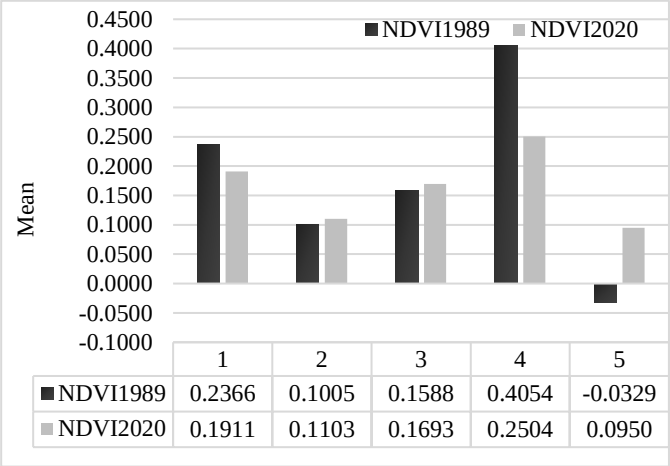

	1	2	3	4	5
NDVI1989	0.2366	0.1005	0.1588	0.4054	-0.0329
NDVI2020	0.1911	0.1103	0.1693	0.2504	0.0950

Figure 7 Simple Bar mean NDVI1989, NDVI2020

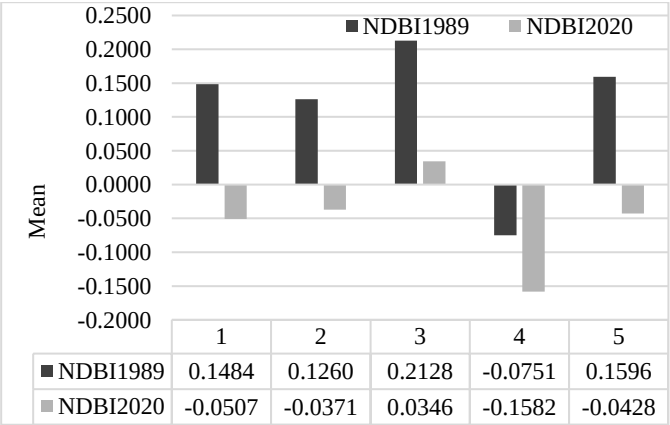

	1	2	3	4	5
NDBI1989	0.1484	0.1260	0.2128	-0.0751	0.1596
NDBI2020	-0.0507	-0.0371	0.0346	-0.1582	-0.0428

Figure 8 Simple Bar Mean NDBI1989, NDBI2020

4.5 Correlation Coefficient between LST among SLOPE, NDVI and NDBI

It is essential to highlight that the correlation between LST and LULC change contributes to the resolution of issues related to human-environment interactions and climate change (Jha et al., 2000). The correlation coefficient (r) matrix from the analysis using SPSS 25 is shown in Table 9. Correlation levels were found in every pair of comparisons at the 0.001 level (2-tailed). The outcome revealed that the NDVI and LST had a lower correlation than the NDBI and LST, which had a higher connection. Conversely, the artificial concrete ground surface emits enormous amounts of LST, whereas the vegetation surface produces less LST (Li et al., 2017). The strength of the relationship between the LST and NDVI was found to be weak or low with the (r) value of -0.356 (1989), and - 0.079 (2020), ($p < 0.001$, 2- tailed).

The result is very consistent with the previous studies (L. Chen et al., 2013; Z. Chen et al., 2020). Simultaneously, the strength of the relationship between LST and NDBI was moderate between 0.5 - 0.7 for all three Landsat images with the (r) value of +0.613, and +0.534, ($p < 0.001$, 2- tailed), for the year 1989, and 2020 respectively. The (r) between LST concerning NDVI value has exhibited a slight increasing trend, whereas between LST and NDBI has shown a slight decrease during the observational period of 1989 to 2020. Whereas the NDVI and NDBI generated an inverse correlation with a value of -0.803 (1989), and -0.799 (2020), the strength of the relationship was very strongly negative. The LST and SLOPE; and SLOPE and NDBI have exhibited a negative correlation, and the correlation coefficient (r) value between the LST and SLOPE was -0.304(1989), and -0.391 (2020), whereas the (r) value between the SLOPE and NDBI was -0.160, -0.143 respectively, and it also indicated that the increasing slope degree leads to the decrease in LST value and NDBI value. Subsequently, a positive relationship was observed between the SLOPE and NDVI, and the (r) value between the SLOPE and NDVI was 0.193 (1989), 0.185 (2020). subsequently indicated that with the increasing SLOPE degree, the NDVI value also increased. Hence, it could be generalized that the vegetation/forest cover areas are significantly increased with the increasing SLOPE value in the study area. The (r) value has also witnessed an increasing trend showing the increase in the quality and health of vegetation cover in the study area. While examining the correlation between NDBI and LST; and NDVI and LST within each LULC class, we also found out that the (r) is not necessarily linear since it may differ between each LULC class, as well as being subject to the different geographical location and season. Therefore, while analysing the accurate LULC and LST relationship, we suggested incorporating the local differences is of utmost importance for a precise conclusion.

4.6 Multiple Linear Regression Model (MLR)

Table 10 exhibited the Model summary of LST, NDVI, Slope, and NDBI obtained using the MLR model; and the MLR model was also used to predict the variable for quantifying LST. Here, the LST is taken as a dependent variable also known as regressand. Whereas NDVI, Slope, and NDBI are taken as independent variables (also known as regressors) for predicting the LST of any given area. The R is a multiple correlation coefficient that is used as a gauge for regressand prediction. The R square denotes the coefficient of determination, and R values of 0.680 and higher denote an adequate prediction level. It displays the percentage of the variance in the dependent variables that the regressors could account for. For the years 1989 and 2020, respectively, the R square values are 0.413 and 0.484. Therefore, as shown in Table 12, NDVI, NDBI, and Slope account for over 41.3 per cent, and 48.4 per cent of the variation in the LST. The overall MLR model was found to be an excellent fit for the provided data by the analysis of variance (ANOVA) shown in Table 11. As the alpha value of 0.05 is more than the significant value of 0.000, the regressors are statistically significant for the prediction of the regressand, F (3, 29521) =6927.57 (1989), and 9227.88 (2020). $p < 0.05$; Correspondingly, it showed that the chosen MLR model fits the data well. The Correlation of the Coefficient Table of LST, NDVI, NDBI, and Slope is shown in Table 13 along with the unstandardized coefficient (B), which illustrates the relationship between the LST and other regressors. In contrast, the negative value of the Slope shows that the LST starts to rise as the Slope begins to fall.

Table 9 Correlations coefficient (r) matrix of LST, NDVI, SLOPE, and NDBI

	LST		NDVI		NDBI		Slope
Parameters	**1989**	**2020**	**1989**	**2020**	**1989**	**2020**	**(SRTM)**
LST 1989	1	.850**	-.356**	-.079**	.613**	.399**	-.304**
LST 2020	.850**	1	-.396**	-.187**	.599**	.534**	-.391**
NDVI 1989	-.356**	-.396**	1	.719**	-.803**	-.740**	.193**
NDVI 2020	-.079**	-.187**	.719**	1	-.422**	-.799**	.185**
NDBI 1989	.613**	.599**	-.803**	-.422**	1	.719**	-.160**
NDBI 2020	.399**	.534**	-.740**	-.799**	.719**	1	-.143**
Slope	-.304**	-.391**	.193**	.185**	-.160**	-.143**	1

**. Correlation is significant at the 0.01 level (2-tailed).

Table:10. Model summary of LST, NDVI, NDBI and Slope

Model Summary				
Model_1989	**R**	**R Square**	**Adjusted R Square**	**Std. Error of the Estimate**
1	.695[a]	0.483	0.482	1.4541
a1. Predictors: (Constant), SLOPE, NDBI1989, NDVI1989				
b1. Dependent Variable: LST1989				
Model_2020	**R**	**R Square**	**Adjusted R Square**	**Std. Error of the Estimate**
3	.762[a]	0.581	0.580	1.3215
a2. Predictors (regressors): (Constant), SLOPE, NDBI2020, NDVI2020				
b2. Dependent Variable (regressand): LST2020				

Table 11. ANOVA summary of LST, NDVI, NDBI and SLOPE.

ANOVA[a]						
Model		**Sum of Squares**	**df**	**Mean Square**	**F**	**Sig.**
1989	**Regression**	2332.73	3	777.58	367.6	.000[b]
	Residual	2496.98	1181	2.114		
	Total	4829.71	1184			
a1. Dependent Variable: LST1989; b1. Predictors: (Constant), SLOPE, NDBI1989, NDVI1989						
2020	**Regression**	2863.27	3	954.42	546.5	.000[b]
	Residual	2062.55	1181	1.746		
	Total	4925.82	1184			
a2. Dependent Variable: LST2020; b2. Predictors: (Constant), SLOPE, NDBI2020, NDVI2020						

Table 12. Correlation of Coefficient table of LST, NDVI, NDBI and Slope.

Coefficients[a]								
Model		Unstandardized Coefficients		Standardized Coefficients	t	Sig.	Collinearity Statistics	
		B	Std. Error	Beta			Tolerance	VIF
1	(Constant) [a]	12.310	0.151		81.408	0.000	-	-
	NDVI1989	4.255	0.435	0.426	12.081	0.000	0.352	2.843
	NDBI1989	11.603	0.444	0.917	26.138	0.000	0.356	2.810
	SLOPE	-0.044	0.004	-0.239	-11.214	0.000	0.963	1.039
2	(Constant) [b]	17.551	0.117		150.437	0.000	-	-
	NDVI2020	17.824	0.761	0.739	23.419	0.000	0.356	2.809
	NDBI2020	27.113	0.793	1.071	34.194	0.000	0.361	2.769
	SLOPE	-0.070	0.004	-0.375	-19.590	0.000	0.966	1.035

a2. Dependent Variable: LST1989[a] and LST2020[b]

Because LST and NDVI correlations are typically positive in the winter and early spring (April) (D. Sun & Kafatos, 2007). The outcome also showed a high NDVI value. The increase in built-up areas is directly related to the rise in LST, according to the positive NDBI value. The positive B value of NDBI shows that an increase in developed land will result in an increase in temperature, proving that LST and NDBI are positively correlated. 1989 = NDVI (t= 48.209, $p < 0.05$), SLOPE (t = -62.198, $p < 0.05$), and NDBI (t = 103.375, $p < 0.05$); 2020 = NDVI (t= 29.691, $p < 0.05$), SLOPE (t = -74.372, $p < 0.05$), and NDBI (t = 98.970, $p < 0.05$) are significant predictors of LST. We concluded that BUAs had a greater impact on the LST based on the size of the t-statistics, which was supported by standardised coefficients. NDVI and NDBI values for LST were derived from Landsat 1989 image. While the MLR model likewise projected that the LST value would decline by 4.7 units for every unit increase in vegetation, it also predicted that the LST value would decline by 0.058 units for every unit increase in slope. The LST would increase by 11 units for every unit increase in the BUAs. The LST, NDVI, and NDBI data gathered from Landsat 2020 images supported the model's prediction that the LST values would decline by 2 units for every unit increase in vegetation and by 0.066 units for every unit increase in slope, respectively. For every unit increase in the BUAs, the LST values would rise by 9 units. As a result, the general form of the equation to forecast LST using Slope, NDBI, and NDVI for the Landsat 1989, and 2020 Landsat image would be as indicated in Table 13 showing the slope, NDBI, LST, and NDVI in respect to the MLR model.

Table 13. Obtained MLR model result between the LST, NDVI, SLOPE and NDBI and the time period, T.

S.N.	Equation	R^2	P value	N
1.	LST_{1989}= 12.310T – (4.255*NDVI) – (-0.044*SLOPE) + (11.603*NDBI)	0.483	0.00	1185
2.	LST_{2020}= 17.551T – (17.824*NDVI) – (-0.070*SLOPE) + (27.113*NDBI)	0.762	0.00	
Predictors: NDVI and NDBI; Dependent variables: LST; Level of Significance ($p < 0.001$)				

5. Conclusion

In the 31-year study period (1989-2020), the analysis investigated the relationships between LST and LULC, NDVI, NDBI, and slope. The research results indicate that the BUAs significantly contribute to the increase in mean LST. Conversely, vegetation cover plays a crucial role in mitigating the impacts of increased LST. Likewise, during the period spanning from 1989 to 2020, BUAs demonstrated a exponential BUAs rise, registering a growth rate of +249.45 per cent, expanding substantially from 44.23 km2 to 154.56 km2. Besides, the responsible predictor of LST and multiple linear regression model and the link between NDVI and LST was found to be minimum, but the correlation between LST and NDBI was moderate in strength. Collectively, the independent factors NDBI, NDVI, and Slope explain 41.3 per cent, and 48.4 per cent of the variation in the LST (dependent variable) in 1989, and 2020, respectively. The analysis of the MLR model explicitly confirmed that the BUAs have become a significant threat to the increase in LST. The study also concluded that additional parameters, such as soil humidity, moisture, etc., should be included in order to improve the MLR model's significance. Moreover, the impact of the LULC class's spatiotemporal variation on LST indicated that the vegetation cover is regularly helping in mean LST decrease and consistently recorded the lowest mean LST among all LULC classes. The result also found that the open scrubland, BUAs and agricultural land were the prime contributors to the mean LST rise. The LST mean and SD value was 14.81°C ± 1.32 in 1989, and it was increased by 18.82°C ± 1.57 in 2020, which showed a tremendous level of rise of 27.07 percent (4.01°C ± 0.125) in the mean LST. Such an increase in LST values is an outcome of the significant level of growth in BUAs and agricultural land, further accelerating the cascading effect of LULC change driven

by anthropogenic activities. The Dehradun Draft Master Plan 2041 which aims to create a sustainable, liveable and dynamic Dehradun city, considering existing infrastructure, land use patterns, environmental factors and proposing solutions for current and future needs. Despite these goals, challenges arise, notably the haphazard growth of BUAs, leading to issues like increasing LST, traffic congestion, air quality decline, and the formation of informal settlements in low-lying areas and seasonal streambeds.

However, to enhance the robustness of the analysis, additional parameters could be incorporated, as the four identified parameters are integral in assessing the counter-magnetic aspect of urbanization, particularly with Built-Up Areas (BUAs) which plays a pivotal role in calculating the other four components: a) BUAs, which involve Geo-spatial database of Dehradun city; b) Creativity Indices encompassing talent, technology, and tolerance indices specific to Dehradun city; c) Reilly's Law of Retail Gravitation to measure the attractiveness of the location and its impact on investor engagement in Dehradun; d) A model of suburban development for Mussoorie; e) Geo-spatial analysis of public transportation accessibility.

Conclusively, as a measures of mitigation, the study recommended that the government create policies that restrict future land encroachment and conversion, notably of forested area and water bodies, and make an immediate effort to increase the quantity and quality of urban vegetation cover in the study area. So that we may, respectively, minimize the potential hazard posed by future LST rise and LULC change.

6. Acknowledgement:

The first author wishes to acknowledge Sufia Rehman (Research Scholar at Jamia Millia Islamia University, New Delhi, India) for her guidance and support. All authors were also highly indebted to the United States Geological Survey (USGS) and Census of India for disseminating Landsat Satellite images and district census handbook data freely available to use.

7. Competing interests

The authors declare that they have no conflict of interest.

8. References:

Aakriti, G., & Ram, B. S. (2015). Analysis of Urban Heat Island (UHI) in Relation to Normalized Difference Vegetation Index (NDVI): A Comparative Study of Delhi and Mumbai. ResearchGate, 2(2). https://doi.org/0.3390/environments2020125

Agarwal, A., Soni, K. K., & Rawat, M. S. S. (2019). Monitoring Land Use Land Cover Change for Dehradun District of Uttarakhand from 2009-2019. International Journal of Advanced Remote Sensing and GIS, 8(1), Article 1.

Ahmad, A., & Quegan, S. (2012). Analysis of Maximum Likelihood classification technique on Landsat 5 TM satellite data of tropical land covers. 2012 IEEE International Conference on Control System, Computing and Engineering, 280–285. https://doi.org/10.1109/ICCSCE.2012.6487156

Amanollahi, J., Tzanis, C., Ramli, M. F., & Abdullah, A. M. (2016). Urban heat evolution in a tropical area utilizing Landsat imagery. Atmospheric Research, 167, 175–182. https://doi.org/10.1016/j.atmosres.2015.07.019

Amiri, R., Weng, Q., Alimohammadi, A., & Alavipanah, S. K. (2009). Spatial–temporal dynamics of land surface temperature in relation to fractional vegetation cover and land use/cover in the Tabriz urban area, Iran. Remote Sensing of Environment, 113(12), 2606–2617. https://doi.org/10.1016/j.rse.2009.07.021

author, D. L. C., Mausel, P., Brondízio, E., & Moran, E. (2004). Change detection techniques. International Journal of Remote Sensing, 25(12), 2365–2401. https://doi.org/10.1080/0143116031000139863

Awuh, M. E., Japhets, P. O., Officha, M. C., Okolie, A. O., & Enete, I. C. (2019). A Correlation Analysis of the Relationship between Land Use and Land Cover/Land Surface Temperature in Abuja Municipal, FCT, Nigeria. Journal of Geographic Information System, 11(1), Article 1. https://doi.org/10.4236/jgis.2019.111004

Balew, A., & Korme, T. (2020). Monitoring land surface temperature in Bahir Dar city and its surrounding using Landsat images. The Egyptian Journal of Remote Sensing and Space Science, 23. https://doi.org/10.1016/j.ejrs.2020.02.001

Bhat, P. A., Shafiq, M. ul, Mir, A. A., & Ahmed, P. (2017). Urban sprawl and its impact on landuse/land cover dynamics of Dehradun City, India. International Journal of Sustainable Built Environment, 6(2), 513–521. https://doi.org/10.1016/j.ijsbe.2017.10.003

Carlson, T. N., & Ripley, D. A. (1997). On the relation between NDVI, fractional vegetation cover, and leaf area index. Remote Sensing of Environment, 62(3), 241–252. https://doi.org/10.1016/S0034-4257(97)00104-1

Çetin, M. (2019). The effect of urban planning on urban formations determining bioclimatic comfort area's effect using satellitia imagines on air quality: A case study of Bursa city. Air Quality, Atmosphere & Health, 12. https://doi.org/10.1007/s11869-019-00742-4

Chamundeeswari, J. (2013). Land Use/ Land Cover Change Detection Using Satellite Remote Sensing and Gis. 17, 1785–1787. https://doi.org/10.5829/idosi.mejsr.2013.17.12.112

Chen, L., Li, M., Huang, F., & Xu, S. (2013). Relationships of LST to NDBI and NDVI in Wuhan City based on Landsat ETM+ image. 2013 6th International Congress on Image and Signal Processing (CISP). https://doi.org/10.1109/CISP.2013.6745282

Chen, Z., Wang, W., & Fu, J. (2020). Vegetation response to precipitation anomalies under different climatic and biogeographical conditions in China. Scientific Reports, 10(1), 830. https://doi.org/10.1038/s41598-020-57910-1

Christopher, B. F., David, B. L., Halton A. Peters, & Nona, R. C. (2007). Feedbacks of Terrestrial Ecosystems to Climate Change | Annual Review of Environment and Resources. 32, 1–29. https://doi.org/10.1146/annurev.energy.32.053006.141119

Darius, P. (2017). Developments in Landsat Land Cover Classification Methods: A Review. 9(9). https://doi.org/10.3390/rs9090967

Dehradun Nagar Nigam. (2018). Population of Proposed Wards of Nagar Nigam Dehradun | District Dehradun | India. https://dehradun.nic.in/document/population-of-proposed-wards-of-nagar-nigam-dehradun/

Deng, Y., Wang, S., Bai, X., Tian, Y., Wu, L., Xiao, J., Chen, F., & Qian, Q. (2018). Relationship among land surface temperature and LUCC, NDVI in typical karst area. Scientific Reports, 8(1), 641. https://doi.org/10.1038/s41598-017-19088-x

Dewan, A. M., Yamaguchi, Y., & Ziaur Rahman, Md. (2012). Dynamics of land use/cover changes and the analysis of landscape fragmentation in Dhaka Metropolitan, Bangladesh. GeoJournal, 77(3), 315–330. https://doi.org/10.1007/s10708-010-9399-x

Fanan, U., Dalama, K. I., & Oluseyi, I. O. (n.d.). Journal of Ecology and The Natural Environment—Urban expansion and vegetal cover loss in and around nigeria's federal capital city. Retrieved December 29, 2020, from https://academicjournals.org/journal/JENE/article-abstract/CE94A3B5892

Fatemi, M., & Narangifard, M. (2019). Monitoring LULC changes and its impact on the LST and NDVI in District 1 of Shiraz City. Arabian Journal of Geosciences, 12(4), 127. https://doi.org/10.1007/s12517-019-4259-6

Fattah, Md. A., Morshed, S. R., & Morshed, S. Y. (2021). Impacts of land use-based carbon emission pattern on surface temperature dynamics: Experience from the urban and suburban areas of Khulna, Bangladesh. Remote Sensing Applications: Society and Environment, 22, 100508. https://doi.org/10.1016/j.rsase.2021.100508

Gandhi, S. M., & Sarkar, B. C. (2016). Chapter 3—Reconnaissance and Prospecting. In S. M. Gandhi & B. C. Sarkar (Eds.), Essentials of Mineral Exploration and Evaluation (pp. 53–79). Elsevier. https://doi.org/10.1016/B978-0-12-805329-4.00010-7

Giri, C., Zhu, Z., & Reed, B. (2005). A comparative analysis of the Global Land Cover 2000 and MODIS land cover data sets. In Remote Sensing of Environment (Vol. 94, Issue 1, p. 10). https://doi.org/10.1016/j.rse.2004.09.005

Goverment of Uttarakhand. (2022, July 22). Climate | District Dehradun | India. https://dehradun.nic.in/climate/

Guha, S., & Govil, H. (2020). Land surface temperature and normalized difference vegetation index relationship: A seasonal study on a tropical city. SN Applied Sciences, 2(10), 1661. https://doi.org/10.1007/s42452-020-03458-8

Guha, S., & Govil, H. (2021). COVID-19 lockdown effect on land surface temperature and normalized difference vegetation index. Geomatics, Natural Hazards and Risk, 12(1), 1082–1100. https://doi.org/10.1080/19475705.2021.1914197

Guha, S., Govil, H., & Diwan, P. (2020a). Monitoring LST-NDVI Relationship Using Premonsoon Landsat Datasets. 2020, 15. https://doi.org/10.1155/2020/4539684

Guha, S., Govil, H., & Diwan, P. (2020b). Monitoring LST-NDVI Relationship Using Premonsoon Landsat Datasets. Advances in Meteorology, 2020, e4539684. https://doi.org/10.1155/2020/4539684

Gupta, K. (n.d.). Unprecedented growth of Dehradun urban area: A spatio-temporal analysis. Retrieved June 23, 2021, from https://www.researchgate.net/publication/282334185_Unprecedented_growth_of_Dehradun_urban_area_a_spatio-temporal_analysis

Hassan, Z., Shabbir, R., Ahmad, S. S., Malik, A. H., Aziz, N., Butt, A., & Erum, S. (2016). Dynamics of land use and land cover change (LULCC) using geospatial techniques: A case study of Islamabad Pakistan. SpringerPlus, 5(1), 812. https://doi.org/10.1186/s40064-016-2414-z

Islam, K., & Islam, S. (2014). Application of Thermal Infrared Remote Sensing to Explore the Relationship between Land Use-Land Cover Changes and Urban Heat Island Effect: A Case Study of Khulna City. 6, 49–60.

Jalan, S., & Sharma, K. (2014). Spatio-temporal Assessment of Land Use/ Land Cover Dynamics and Urban Heat Island of Jaipur City using Satellite Data. XL(8). https://doi.org/10.5194/isprsarchives-XL-8-767-2014

Jana, C., Mandal, D., Shrimali, S. S., Alam, N. M., Kumar, R., Sena, D. R., & Kaushal, R. (2020a). Assessment of urban growth effects on green space and surface temperature in Doon Valley, Uttarakhand, India. Environmental Monitoring and Assessment, 192(4), 257. https://doi.org/10.1007/s10661-020-8184-7

Jana, C., Mandal, D., Shrimali, S. S., Alam, N. M., Kumar, R., Sena, D. R., & Kaushal, R. (2020b). Assessment of urban growth effects on green space and surface temperature in Doon Valley, Uttarakhand, India.

Environmental Monitoring and Assessment, 192(4), 257. https://doi.org/10.1007/s10661-020-8184-7

J.C., P. (1990). Using spatial context in satellite data to infer regional scale evapotranspiration—IEEE Journals & Magazine. 28(5), 940–948. https://doi.org/10.1109/36.58983.

Jenness, J., & Wynne, J. J. (2005). Cohen's Kappa and classification table metrics 2.0: An ArcView 3.x extension for accuracy assessment of spatially explicit models. Open-File Report OF 2005-1363. Flagstaff, AZ: U.S. Geological Survey, Southwest Biological Science Center. 86 p. https://www.fs.usda.gov/treesearch/pubs/25707

Jha, C. S., Dutt, C. B. S., & Bawa, K. S. (2000). Deforestation and land use changes in Western Ghats, India. Current Science, 79(2), 231–238.

Kumar, R., Mishra, V., Buzan, J., Kumar, R., Shindell, D., & Huber, M. (2017). Dominant control of agriculture and irrigation on urban heat island in India. Scientific Reports, 7(1), Article 1. https://doi.org/10.1038/s41598-017-14213-2

Landis, J. R., & Koch, G. G. (1977). The measurement of observer agreement for categorical data. Biometrics, 33(1), 159–174.

Li, W., Cao, Q., Lang, K., & Wu, J. (2017). Linking potential heat source and sink to urban heat island: Heterogeneous effects of landscape pattern on land surface temperature. The Science of the Total Environment, 586, 457–465. https://doi.org/10.1016/j.scitotenv.2017.01.191

Lillesand, T., Kiefer, R. W., & Chipman, J. (2015). Remote Sensing and Image Interpretation. John Wiley & Sons.

Liu, L., & Zhang, Y. (2011). Urban Heat Island Analysis Using the Landsat TM Data and ASTER Data: A Case Study in Hong Kong. Remote Sensing, 3(7), Article 7. https://doi.org/10.3390/rs3071535

Lo, C. P., & Quattrochi, D. (2003). Land-Use and Land-Cover Change, Urban Heat Island Phenomenon, and Health Implications: A Remote Sensing Approach. Photogrammetric Engineering & Remote Sensing, 69, 1053–1063. https://doi.org/10.14358/PERS.69.9.1053

Lu, L., Weng, Q., Xiao, D., Guo, H., Li, Q., & Hui, W. (2020). Spatiotemporal Variation of Surface Urban Heat Islands in Relation to Land Cover Composition and Configuration: A Multi-Scale Case Study of Xi'an, China. Remote Sensing, 12(17), Article 17. https://doi.org/10.3390/rs12172713

Lv, Z., Liu, T., Zhang, Benediktsson, J. A., & Chen, Y. (2018). Land Cover Change Detection Based on Adaptive Contextual Information Using Bi-Temporal Remote Sensing Images. 10(6), 901. https://doi.org/10.3390/rs10060901

Macarof, P., & Florian, S. (2017). Comparasion of NDBI and NDVI as Indicators of Surface Urban Heat Island Effect in Landsat 8 Imagery: A Case Study of Iasi. Present Environment and Sustainable Development, 11. https://doi.org/10.1515/pesd-2017-0032

Malik, M. S., Shukla, J., & Mishra, S. N. (2019). Relationship of LST, NDBI and NDVI using landsat-8 data in Kandaihimmat watershed, Hoshangabad, India. Indian Journal of Geo-Marine Sciences, 48, 25–31.

Mallick, J., Kant, Y., & Bharath, B. D. (n.d.). Estimation of land surface temperature over Delhi using Landsat-7 ETM+. Retrieved December 30, 2020, from https://www.researchgate.net/publication/228895796_Estimation_of_land_surface_temperature_over_Delhi_using_Landsat-_ETM

Mishra, P. K., Rai, A., & Rai, S. C. (2020). Land use and land cover change detection using geospatial techniques in the Sikkim Himalaya, India. The Egyptian Journal of Remote Sensing and Space Science, 23(2), 133–143. https://doi.org/10.1016/j.ejrs.2019.02.001

Morshed, S. R., Fattah, Md. A., Haque, Md. N., & Morshed, S. Y. (2022). Future ecosystem service value modeling with land cover dynamics by using machine learning based Artificial Neural Network model for Jashore city, Bangladesh. Physics and Chemistry of the Earth, Parts A/B/C, 126, 103021. https://doi.org/10.1016/j.pce.2021.103021

Naidoo, U., Flack, P., & Essack, S. (2013). Secondary school factors relating to academic success in first year School of Health Science students at the University of KwaZulu-Natal.

Naif, S. S., Mahmood, D. A., & Al-Jiboori, M. H. (2020). Seasonal normalized difference vegetation index responses to air temperature and precipitation in Baghdad. Open Agriculture, 5(1), 631–637. https://doi.org/10.1515/opag-2020-0065

Nichol, J. E., & To, P. H. (2012). Temporal characteristics of thermal satellite images for urban heat stress and heat island mapping. ISPRS Journal of Photogrammetry and Remote Sensing, 74, 153–162. https://doi.org/10.1016/j.isprsjprs.2012.09.007

Nzoiwu, C. P., Agulue, E. I., Mbah, S., & Igboanugo, C. P. (2017). Impact of Land Use/Land Cover Change on Surface Temperature Condition of Awka Town, Nigeria. Journal of Geographic Information System, 9(6), Article 6. https://doi.org/10.4236/jgis.2017.96047

Pal, S., & Ziaul, Sk. (2017a). Detection of land use and land cover change and land surface temperature in English Bazar urban centre. The Egyptian Journal of Remote Sensing and Space Science, 20(1), 125–145. https://doi.org/10.1016/j.ejrs.2016.11.003

Pal, S., & Ziaul, Sk. (2017b). Detection of land use and land cover change and land surface temperature in English Bazar urban centre. The Egyptian Journal of Remote Sensing and Space Science, 20(1), 125–145. https://doi.org/10.1016/j.ejrs.2016.11.003

Patidar, S., & Sankhla, V. (2015). Change Detection of Land-use and Land-cover of Dehradun City: A Spatio-Temporal Analysis. https://doi.org/10.23953/CLOUD.IJARSG.105

Reisi, M., Ahmadi Nadoushan, M., & Aye, L. (2019). Remote sensing for urban heat and cool islands evaluation in semi-arid areas. Global Journal of Environmental Science and Management, 5(3), 319–330. https://doi.org/10.22034/GJESM.2019.03.05

Rogan, J., & Chen, D. (2004). Remote sensing technology for mapping and monitoring land-cover and land-use change. Progress in Planning, 4(61), 301–325. https://doi.org/10.1016/S0305-9006(03)00066-7

Rouse, J., Haas, R. H., Schell, J. A., & Deering, D. (1973). Monitoring vegetation systems in the great plains with ERTS. Undefined. https://www.semanticscholar.org/paper/Monitoring-vegetation-systems-in-the-great-plains-Rouse-Haas/fb2f60fe0fe2874e5cbf927a2556d719c32eac29

Saini, V., & Tiwari, R. (2017, October 23). EFFECT OF URBANIZATION ON LAND SURFACE TEMPERATURE AND NDVI: A CASE STUDY OF DEHRADUN, INDIA.

Santosa, P. B. (2016). Evaluation of satellite image correction methods caused by differential terrain illumination. *Jurnal Forum Geografi. Vol. 30, No. 1 (2016).* https://doi.org/10.23917/forgeo.v30i1.1768

Shalaby, A., & Tateishi, R. (2007). Remote sensing and GIS for mapping and monitoring land cover and land-use changes in the Northwestern coastal zone of Egypt, Appl. Applied Geography, 27, 28–41. https://doi.org/10.1016/j.apgeog.2006.09.004

Singh, P., Kikon, N., & Verma, P. (2017). Impact of land use change and urbanization on urban heat island in Lucknow city, Central India. A remote sensing based estimate. Sustainable Cities and Society, 32, 100–114. https://doi.org/10.1016/j.scs.2017.02.018

Sobrino, J. A., Raissouni, N., & Li, Z.-L. (2001). A Comparative Study of Land Surface Emissivity Retrieval from NOAA Data. Remote Sensing of Environment, 75(2), 256–266. https://doi.org/10.1016/S0034-4257(00)00171-1

Sobrino, J., Jimenez-Munoz, J.-C., & Paolini, L. (2004). Land surface temperature retrieval from LANDSAT TM 5. Remote Sensing of Environment, 90, 434–440. https://doi.org/10.1016/j.rse.2004.02.003

Sobrino, J., Raissouni, N., & Li, Z.-L. (2001). A Comparative Study of Land Surface Emissivity Retrieval from NOAA Data. Remote Sensing of Environment, 75, 256–266. https://doi.org/10.1016/S0034-4257(00)00171-1

Song, J., Du, S., Feng, X., & Guo, L. (2014). The relationships between landscape compositions and land surface temperature: Quantifying their resolution sensitivity with spatial regression models. Landscape and Urban Planning, 123, 145–157. https://doi.org/10.1016/j.landurbplan.2013.11.014

Sresto, M. A., Siddika, S., Fattah, Md. A., Morshed, S. R., & Morshed, Md. M. (2022a). A GIS and remote sensing approach for measuring summer-winter variation of land use and land cover indices and surface temperature in Dhaka district, Bangladesh. Heliyon, 8(8), e10309. https://doi.org/10.1016/j.heliyon.2022.e10309

Sresto, M. A., Siddika, S., Fattah, Md. A., Morshed, S. R., & Morshed, Md. M. (2022b). A GIS and remote sensing approach for measuring summer-winter variation of land use and land cover indices and surface temperature in Dhaka district, Bangladesh. Heliyon, 8(8), e10309. https://doi.org/10.1016/j.heliyon.2022.e10309

Srivastava, P. K., Han, D., Rico-Ramirez, M. A., Bray, M., & Islam, T. (2012). Selection of classification techniques for land use/land cover change investigation. Advances in Space Research, 50(9), 1250–1265. https://doi.org/10.1016/j.asr.2012.06.032

Stehman, S. V., & Czaplewski, R. L. (1998). Design and Analysis for Thematic Map Accuracy Assessment: Fundamental Principles. 64, 331–344.

Sun, D., & Kafatos, M. (2007). Note on the NDVI-LST relationship and the use of temperature-related drought indices over North America. Geophysical Research Letters, 34(24). https://doi.org/10.1029/2007GL031485

Sun, L., Liang, S., Yuan, W., & Chen, Z. (2013). Improving a Penman–Monteith evapotranspiration model by incorporating soil moisture control on soil evaporation in semiarid areas. International Journal of Digital Earth, 6(sup1), 134–156. https://doi.org/10.1080/17538947.2013.783635

Sun, Q., Wang, Z., Li, Z., Erb, A., & Schaaf, C. B. (2017). Evaluation of the global MODIS 30 arc-second spatially and temporally complete snow-free land surface albedo and reflectance anisotropy dataset. International Journal of Applied Earth Observation and Geoinformation, 58, 36–49. https://doi.org/10.1016/j.jag.2017.01.011

Syafitri, A. K. N., & Santosa, P. B. (2020). Spatial Analysis of Kulon Progo District Development from 2007-2030 with Cellular Automata Markov Model. *Proceeding The 1st International Conference on Geodesy, Geomatics, and Land Administration 2019. KnE Engineering, 4(3), 269–277.* https://doi.org/10.18502/keg.v4i3.5864

Taloor, A. K., Kumar, V., Singh, V. K., Singh, A. K., Kale, R. V., Sharma, R., Khajuria, V., Raina, G., Kouser, B., & Chowdhary, N. H. (2020). Land Use Land Cover

Dynamics Using Remote Sensing and GIS Techniques in Western Doon Valley, Uttarakhand, India. In S. Sahdev, R. B. Singh, & M. Kumar (Eds.), Geoecology of Landscape Dynamics (pp. 37–51). Springer. https://doi.org/10.1007/978-981-15-2097-6_4

Thakur, S., Mondal, I., Ghosh, P. B., Das, P., & De, T. K. (2020). A review of the application of multispectral remote sensing in the study of mangrove ecosystems with special emphasis on image processing techniques. Spatial Information Research, 28(1), 39–51. https://doi.org/10.1007/s41324-019-00268-y

Thapa, R., & Bahuguna, V. (2021). Monitoring Land Encroachment and Land Use & Land Cover (LULC) Change in The Pachhua Dun, Dehradun District Using Landsat Images 1989 and 2020. JGISE: Journal of Geospatial Information Science and Engineering, 4, 71. https://doi.org/10.22146/jgise.64857

Thomlinson, J. R., Bolstad, P. V., & Cohen, W. B. (1999). Coordinating Methodologies for Scaling Landcover Classifications from Site-Specific to Global: Steps toward Validating Global Map Products. Remote Sensing of Environment, 70(1), 16–28. https://doi.org/10.1016/S0034-4257(99)00055-3

Verma, P., Raghubanshi, A., Srivastava, P. K., & Raghubanshi, A. S. (2020). Appraisal of kappa-based metrics and disagreement indices of accuracy assessment for parametric and nonparametric techniques used in LULC classification and change detection. Modeling Earth Systems and Environment, 6(2), 1045–1059. https://doi.org/10.1007/s40808-020-00740-x

Walsh, S. J., Crawford, T. W., Welsh, W. F., & Crews-Meyer, K. A. (2001). A multiscale analysis of LULC and NDVI variation in Nang Rong district, northeast Thailand. Agriculture, Ecosystems & Environment, 85(1), 47–64. https://doi.org/10.1016/S0167-8809(01)00202-X

Weng, Q., Lu, D., & Schubring, J. (2004). Estimation of land surface temperature–vegetation abundance relationship for urban heat island studies. Remote Sensing of Environment, 89(4), 467–483. https://doi.org/10.1016/j.rse.2003.11.005

Xiaoqing, Z., & Jianlan, R. (2007). Study on Dynamic Mechanism of Urban Expansion: A Case Study of Shandong Province. Chinese Journal of Population Resources and Environment, 5(3), 37–42. https://doi.org/10.1080/10042857.2007.10677516

Yim, K. H., Nahm, F. S., Han, K. A., & Park, S. Y. (2010). Analysis of Statistical Methods and Errors in the Articles Published in the Korean Journal of Pain. 23(1), 35–41. https://doi.org/10.3344/kjp.2010.23.1.35

Yusuf, Y. A., Pradhan, B., & Idrees, M. O. (2014). Spatio-temporal Assessment of Urban Heat Island Effects in Kuala Lumpur Metropolitan City Using Landsat Images. Journal of the Indian Society of Remote Sensing, 42(4), 829–837. https://doi.org/10.1007/s12524-013-0342-8

Yuvaraj, R. M. (2020). Extents of Predictors for Land Surface Temperature Using Multiple Regression Model. The Scientific World Journal, 2020, e3958589. https://doi.org/10.1155/2020/3958589

Zha, Y., Gao, J., & Ni, S. (2003). Use of normalized difference built-up index in automatically mapping urban areas from TM imagery. International Journal of Remote Sensing, 24(3), 583–594. https://doi.org/10.1080/01431160304987

Zhang, F., Tiyip, T., Kung, H., Johnson, V. C., Maimaitiyiming, M., Zhou, M., & Wang, J. (2016). Dynamics of land surface temperature (LST) in response to land use and land cover (LULC) changes in the Weigan and Kuqa river oasis, Xinjiang, China. Arabian Journal of Geosciences, 9(7), 499. https://doi.org/10.1007/s12517-016-2521-8

Zhang, Y., Odeh, I. O. A., & Ramadan, E. (2013). Assessment of land surface temperature in relation to landscape metrics and fractional vegetation cover in an urban/peri-urban region using Landsat data. International Journal of Remote Sensing, 34(1), 168–189. https://doi.org/10.1080/01431161.2012.712227

Zhou, X., & Wang, Y.-C. (2011a). Dynamics of Land Surface Temperature in Response to Land-Use/Cover Change. Geographical Research, 49(1), 23–36. https://doi.org/10.1111/j.1745-5871.2010.00686.x

Zhou, X., & Wang, Y.-C. (2011b). Dynamics of Land Surface Temperature in Response to Land-Use/Cover Change. Geographical Research, 49(1), 23–36. https://doi.org/10.1111/j.1745-5871.2010.00686.x